JACS
JOURNAL OF THE AMERICAN CHEMICAL SOCIETY

Article

Cite This: *J. Am. Chem. Soc.* 2019, 141, 13074−13080

pubs.acs.org/JACS

Asynchronous Photoexcited Electronic and Structural Relaxation in Lead-Free Perovskites

Cunming Liu,[†] Yingqi Wang,[§] Huifang Geng,[⊥] Taishan Zhu,[$] Elif Ertekin,[$] David Gosztola,[‡] Sizhuo Yang,[&] Jier Huang,[&] Bin Yang,[∇] Keli Han,[∇] Sophie E. Canton,[⊥,¶] Qingyu Kong,[○] Kaibo Zheng,[*,¥,☆] and Xiaoyi Zhang[*,†]

[†]X-ray Science Division, and [‡]Center for Nanoscale Materials, Argonne National Laboratory, 9700 S. Cass Avenue, Lemont, Illinois 60439, United States

[§]Center for High Pressure Science and Technology Advanced Research, Shanghai 201203, China

[⊥]ELI-ALPS, ELI-HU Non-Profit, Ltd., Dugonics ter 13, Szeged 6720, Hungary

[$]Department of Mechanical Science and Engineering, University of Illinois at Urbana−Champaign, 1206 West Green Street, Urbana, Illinois 61801, United States

[&]Department of Chemistry, Marquette University, Milwaukee, Wisconsin 53201, United States

[∇]State Key Laboratory of Molecular Reaction Dynamics, Dalian Institute of Chemical Physics, Chinese Academy of Science, Dalian, China

[¶]Deutsches Elektronen Synchrotron (DESY), Notkestrasse 85, D-22607 Hamburg, Germany

[○]Sychrotron Soleil, L'Orme des Merisiers St Aubin, F-91192 Gif-sur-Yvette, France

[¥]Department of Chemical Physics and Nanolund, Lund University, Box 124, 22100 Lund, Sweden

[☆]Department of Chemistry, Technical University of Denmark, DK-2800 Kongens Lyngby, Denmark

Supporting Information

ABSTRACT: Vacancy-ordered lead-free perovskites with more-stable crystalline structures have been intensively explored as the alternatives for resolving the toxic and long-term stability issues of lead halide perovskites (LHPs). The dispersive energy bands produced by the closely packed halide octahedral sublattice in these perovskites are meanwhile anticipated to facility the mobility of charge carriers. However, these perovskites suffer from unexpectedly poor charge carrier transport. To tackle this issue, we have employed the ultrafast, elemental-specific X-ray transient absorption (XTA) spectroscopy to directly probe the photoexcited electronic and structural dynamics of a prototypical vacancy-ordered lead-free perovskite ($Cs_3Bi_2Br_9$). We have discovered that the photogenerated holes quickly self-trapped at Br centers, simultaneously distorting the local lattice structure, likely forming small polarons in the configuration of V_k center (Br_2^- dimer). More significantly, we have found a surprisingly long-lived, structural distorted state with a lifetime of ~59 μs, which is ~3 orders of magnitude slower than that of the charge carrier recombination. Such long-lived structural distortion may produce a transient "background" under continuous light illumination, influencing the charge carrier transport along the lattice framework.

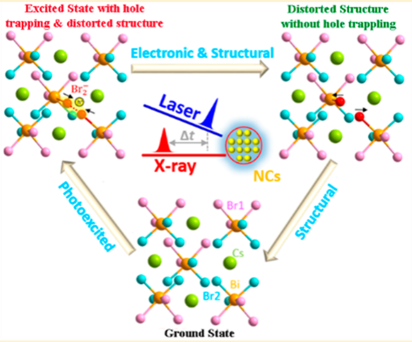

INTRODUCTION

Lead halide perovskite (LHP)-based solar cells have received immense attention in recent years, because of their low cost and superior power conversion efficiency.[1−4] However, the commercialization of LHP solar cells is currently limited by the potential environmental and public health concerns, which result from the toxicity of water-soluble, unstable lead salts under ambient conditions.[5,6] The vacancy-ordered lead-free perovskites, such as Sn- or Te-based double perovskites,[7−9] and Bi- or Sb-based two-dimensional (2D) layered perovskites, as well as their zero-dimensional (0D) ones,[9−12] have been explored as low/nontoxic replacements for LHPs, because of their stabilized crystalline lattice structures. Although the octahedral connectivity in these perovskites is reduced, the closely packed halide octahedral sublattice is still anticipated to provide dispersive energy bands for good charge carrier mobility.[13] However, the power conversion efficiency of such perovskite-based devices is far below expectations.[9,12,14]

Photoexcitation of LHPs with energy above the bandgap creates the charge carriers, namely, electrons (e^-) and holes (h^+). The photogenerated charge carriers might be trapped,

Received: April 28, 2019
Published: July 30, 2019

DOI: 10.1021/jacs.9b04557
J. Am. Chem. Soc. 2019, 141, 13074−13080

accompanied by lattice distortion due to the strong carrier–phonon interaction.[15−20] This process is known as polaron formation, and it has been recently used to rationalize the intrinsic origin of the success of LHPs in photovoltaic applications. Nonetheless, the conclusion of polaron formation is mainly derived or speculated through indirect experiments or calculations.[15−20] Hence, direct experimental observation of the electronic and structural dynamics correlated with polaron formation and relaxation is crucial in uncovering the fundamentally photophysical mechanisms of perovskite materials. Recently, we have directly observed the photoinduced electron polaron formation in an LHP.[21] However, knowledge of polaron formation in lead-free perovskites is largely missing, despite of its great importance.

Herein, using the ultrafast, elemental-specific X-ray transient absorption (XTA) spectroscopy (see the description of the technique given in the Supporting Information and the setup schematic shown in Figure S1 in the Supporting Information), we directly visualized the photoinduced electronic and structural dynamics of a prototypical vacancy-ordered, lead-free perovskite: $Cs_3Bi_2Br_9$ (space group $P\bar{3}m1$, a = 7.972 Å and c = 9.867 Å), in the form of ∼3.8 nm nanocrystals (NCs) (see Figures S2 and S3 in the Supporting Information), which were prepared by a modified one-step reaction method (see details in the Supporting Information).[22] The NCs exhibit a strong exciton peak at 2.84 eV in their UV-vis absorption spectrum, because of their own natural quantum wells caused by their vacancy-ordered 2D-layered structures (see Figures S2b and S3b in the Supporting Information) and each NC is composed of ∼54 unit cells (see the calculations in the Supporting Information). Our experimental results evidence the photoinduced small polaron formation in $Cs_3Bi_2Br_9$ NCs, in which the photoexcited hole is fast self-trapped (<10 ps) at the Br ions, distorting the Br local lattice structure. Surprisingly, we have observed an ultra-long-lived structural distorted intermediate state (∼59 us), which is 3 orders of magnitude slower than the recombination (∼20 ns) between the electrons and self-trapped holes. Our findings here represent a step forward in uncovering fundamental mechanistic details on the electronic and structural response of the photoinduced polaron state in perovskite materials.

■ RESULTS AND DISCUSSION

In consideration of the ∼120 ps time resolution of the XTA spectroscopic technique here, femtosecond optical transient absorption (fs-OTA) spectroscopy (detailed in the Supporting Information) was first performed to measure the early time relaxation dynamics of photoexcited charge carriers (e^- and h^+), using 120 fs laser pulses of 3.1 eV as the pump and broadband 120 fs visible pulses as the probe. According to the electronic density of states (EDOS) (Figure 1a) projected from the band structure (Figure S4 in the Supporting Information) of bulk $Cs_3Bi_2Br_9$ perovskite calculated by density functional theory (DFT), the laser photons excite the electrons in the valence band (VB) that is primarily composed of Br 4p orbitals to the conduction band (CB) majorly contributed by Bi 6p orbitals hybridized with a small amount of Br 4p orbitals (Bi 6p/Br 4p hybrid). Figure 1b shows the normalized charge carrier kinetics by monitoring the photobleaching recovery of exciton state at 2.84 eV (Figure S5a in the Supporting Information), under the laser pump flux J_0 from 1.9×10^{13} photons/cm^2 ($\langle N_0\rangle$ = 0.02) to 5.6×10^{15} photons/cm^2 ($\langle N_0\rangle$ = 6.7), where $\langle N_0\rangle$ is the averaged number of

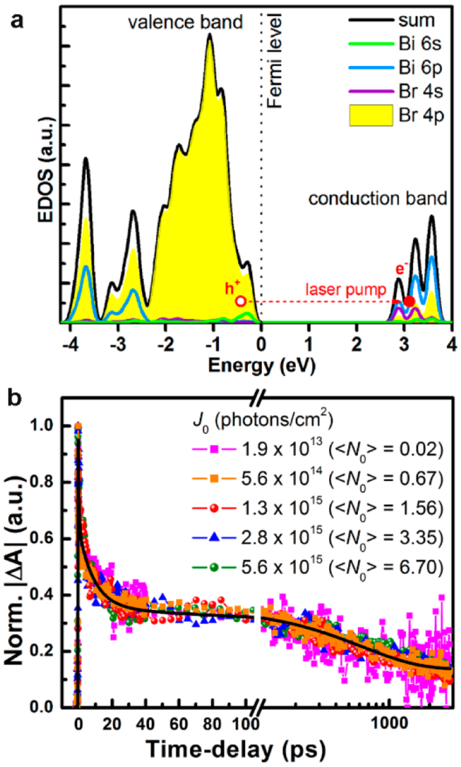

Figure 1. (a) Electronic density of states (EDOS) for $Cs_3Bi_2Br_9$ bulk obtained through DFT calculations, indicating the atomic orbital compositions of valence and conduction band structure. (b) Normalized fs-OTA kinetics for photobleaching recovery of the exciton state probed at 2.84 eV under different laser pump flux, fitted by a multiple-exponential model convoluted with Gaussian instrument response function (IRF) of ∼140 fs (fwhm) (black curve).

photons per nanoparticle (see details in the Supporting Information). The decay kinetics here does not vary with the laser pump flux, implying an insignificant Auger recombination effect, which can be further confirmed by the linear power-dependent amplitudes of exciton state photobleaching at time delays of 1 ps, 90 ps, and 1 ns (see Figure S5b in the Supporting Information). The fitting of these decay curves with a multiple-exponential decay model reveals three lifetime components of 0.5 ± 0.1 ps (44%), 9.3 ± 0.7 ps (32%), and 628 ± 37 ps (24%) for charge carrier relaxation dynamics, assignments of which would be discussed with XTA results later.

While OTA spectroscopy provides valuable information on the charge carrier dynamics, it cannot ambiguously distinguish the contribution from different types of charge carriers (e^- and h^+) or from different atomic centers. Nor can it track the excited state that does not possess transition strength over the laser spectrum range, which is referred as the optically dark state. The intrinsic, element-specific, oxidation state and local structure sensitive characteristics of XTA technique enable it as an ideal tool to interrogate how charge carriers flow inside the perovskite, as well as distort the local lattice structure. The XTA measurements were performed using ∼1.6 ps laser pulses of 3.1 eV as the pump and 120 ps X-ray pulse train from a synchrotron source as the probe (see Figure S1). Figure 2a shows Br K-edge X-ray absorption (XA) spectra of NCs in the ground state (GS) ($\mu(E)$, black curve) and at the time delay (Δt) of 90 ps (red curve) after laser excitation. The Br K-edge absorption measures the transition from the Br 1s orbital to

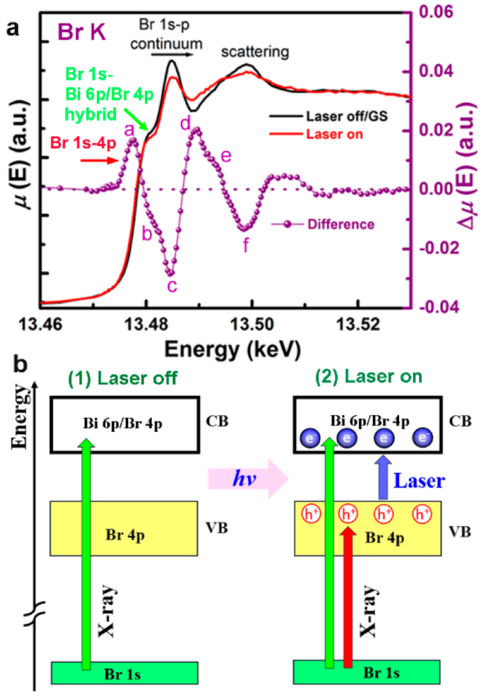

Figure 2. (a) XA spectra (μ(E)) at Br K before laser excitation (laser-off/GS, black curve) and after laser excitation (laser-on at Δt = 90 ps, red curve) (5.6×10^{16} photons/cm^2). The XTA spectrum is the difference between XA spectra with the laser on and the laser off. (b) Schematic of Br K near-edge transitions before laser excitation (1) and after laser excitation (2).

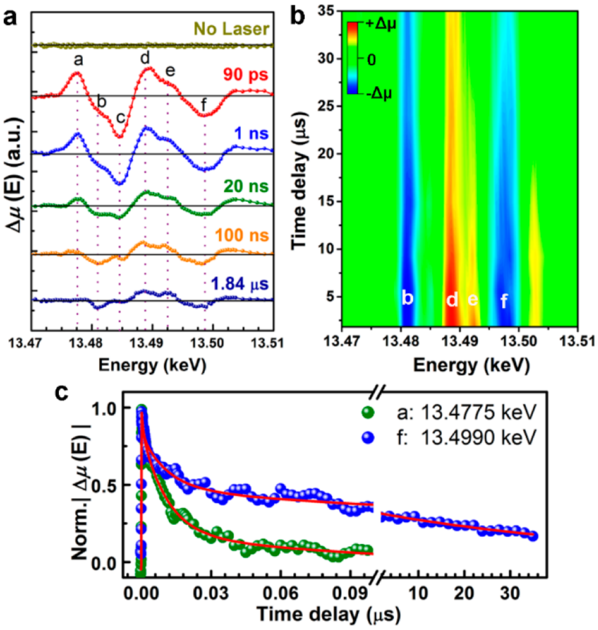

Figure 3. (a) Br K-edge XTA spectra under several representative early time delays. (b) 2D XTA spectra between 1.84 and 35 μs. (c) XTA kinetics measured at the representative energies for hole self-trapped (green curve) and structure distortion (blue curve). The red curves are multiple-exponential fits convoluted with a Gaussian IRF of ~120 ps (fwhm).

upper unoccupied orbitals and the continuum with *p*-characteristics.[23,24] Thus, we can attribute the shoulder peak at the left side of the main edge absorption peak (13.4844

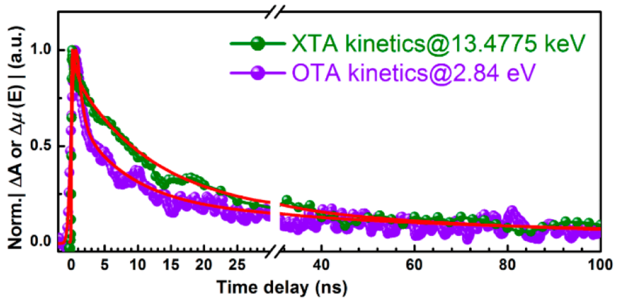

Figure 4. Complete photoexcited charge carrier recombination dynamics measured by monitoring the recovery of exciton state photobleaching at 2.84 eV using ns-OTA spectroscopy (purple dots) at 2.8×10^{15} photons/cm^2, which is compared to that (green dots) measured from the XTA kinetics by probing at 13.4775 keV for the hole relaxation at the Br site at 5.6×10^{16} photons/cm^2.

keV), centered at ~13.4802 keV, to the transition from the Br 1s orbital to the bottom of the empty conduction band, namely, the Bi 6p (major)/Br 4p (minor) hybridized state (see Figure 2b(1)). This assignment has been further confirmed by ORCA calculation (see Figure S6 in the Supporting Information). The main edge absorption transition that peaked at 13.4844 keV is due to the Br 1s to *p* continuum transition (called the X-ray absorption white line). The peak at ~13.499 keV in the GS XA spectrum (Figure 2a, black curve) is caused by the scattering of X-ray created photoelectrons by the neighboring atoms around the Br atoms, directly reflecting the local geometric structure around Br sites.[23,24]

Similar XTA measurements were conducted at the Bi L$_3$-edge (Bi 2p$_{3/2}$ orbital to upper unoccupied orbitals and a continuum with *d*-characteristics) to detect the photoexcited electrons. The results showed no detectable difference absorption between with and without laser excitation within the experimental resolution even by doubling the laser photon flux as used in Br K-edge measurements (see Figure S7 in the Supporting Information). Further increasing the laser power leads to the fast photodegradation of NCs. One possible explanation for this is that most of the photogenerated electrons are highly deviated from Bi cations by the strong coulomb interaction of the hole self-trapped at Br anions, which is also indicated by the prominent exciton peak in the UV-vis spectrum (see Figure S2d in the Supporting Information). This finding agrees with the observation of electron delocalization from Pb site that is obtained by measuring the Pb L$_3$-edge aborption of $CsPbBr_3$ NCs.[25]

To better illustrate the XA change before and after laser excitation, the XTA spectrum obtained by subtracting $\mu(E)_{GS}$ from $\mu(E)_{laser\text{-}on}$ (Δt = 90 ps) was also shown in Figure 2a (purple curve). The main features in the XTA spectrum were indicated by labels "(a)"−"(f)". The sharp positive feature "(a)" before the shoulder peak (13.4802 keV) in the GS XA spectrum indicates that the photoexcitation induces an extra Br 1s-to-p transition (13.4775 keV). As laser photons pump the electrons from the VB to the CB, the Br 4p holes are created in the VB, resulting in an extra XA transition of Br 1s electrons to 4p holes in the VB (Figure 2b(2)), which is shown as feature "(a)" in the XTA spectrum. Such a transition does not exist in the GS XA spectrum, because the VB is fully occupied by the electrons in the GS (Figure 2b(1)). Therefore, feature "(a)" directly reflects the photocreated hole density at Br atom centers. Since features "(e)" and "(f)" correspond to the

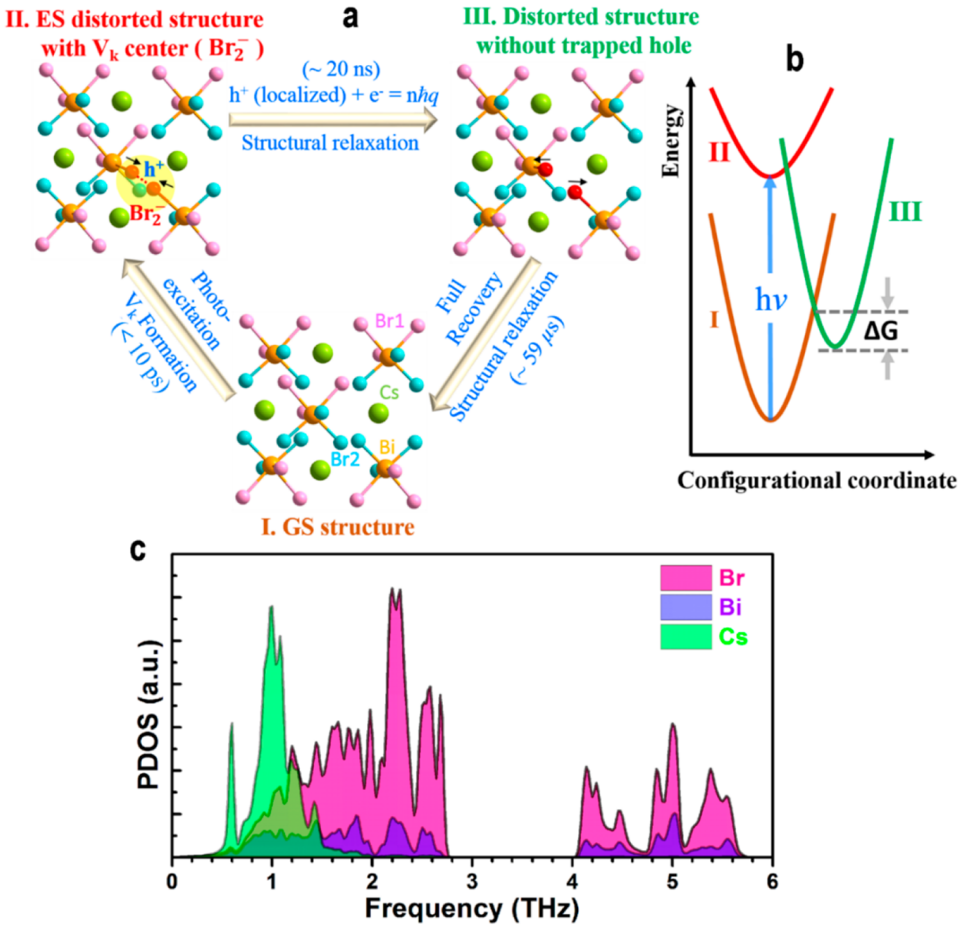

Figure 5. (a) Schematic photocycle of $Cs_3Bi_2Br_9$ NCs. (b) Schematic configuration−coordinate potential-energy diagram representing the relative energies of states (I), (II), and (III) shown in Figure 5a. The energy difference between states (II) and (I) is 2.84 eV, and the estimated energy barrier Δ*G* between states (III) and (II) is 0.485 eV. (c) Calculated phonon density of states (PDOS) of Br, Bi, and Cs atoms versus their vibration frequencies in $Cs_3Bi_2Br_9$ bulk for understanding the slow structural distortion recovery.

scattering peak in the GS spectrum, they can be mainly associated with the photoinduced local structural change around Br atoms. Features "(b)", "(c)", and "(d)" first show the reduction and then the increase of Br 1s to the CB Bi 6p/Br 4p and *p* continuum transitions, indicating that both transitions shift to higher energies. The photoexcitation reduces the electron density at Br centers so that it lowers the electronic screening effect, resulting in the increase of absorption edge energies. The edge energies are sensitive to both the oxidation state and the local structure, which are often coupled together, showing a combination effect of both in the near-edge region.[26−28] Therefore, it is difficult to separate the charge and structure effects on features "(b)"−"(d)".

Figure 3a shows a series of Br K-edge XTA spectra collected at early Δ*t*, ranging from 90 ps to 1.84 μs. Feature "(a)", which reflects photoexcited holes trapped at Br centers, quickly decreases and almost disappears at Δ*t* = 100 ns. By contrast, features "(e)" and "(f)" that are mainly associated with the local structural change clearly exist at Δ*t* = 1.84 μs and are still present at Δ*t* = 35 μs (Figure 3b). This implies that the small local structural distortion exists even after Br 4p holes in the valence band are recombined by the electrons. The shape of the XTA spectra after 100 ns shows no detectable changes (see Figure S7), suggesting only one intermediate state over the μs-scale delay range. In order to quantitatively extract the time scales for relaxation dynamics of the self-trapped holes and for the recovery dynamics of the local structural distortion around Br atoms, the XTA kinetics were measured at two peaks: "(a)" and "(f)", which are fingerprints for hole self-trapping and structural distortion, respectively. These two kinetics (Figure 3c) are very similar in the first 5 ns but grow apart later. The fitting of kinetics probed at the peak "(a)" by the multiple-exponential function convoluted with Gaussian instrument response function (IRF) of ~120 ps (fwhm) reveal three lifetime components: 628 ± 37 ps (15%), 11.4 ± 1.1 ns (70%), and 81.0 ± 4.2 ns (15%), giving an amplitude-averaged lifetime of 20.2 ± 1.0 ns. The lifetime component of ~628 ps for self-trapped hole relaxation has also been captured by fs-OTA, which indicates that hole tapping must happen prior to this, in the hot carrier thermalization processes of ~0.5 ps or ~9.3 ps measured in fs-OTA (Figure 1b) or earlier. In other words, the hole is fast localized at the Br atom in the time scale of <10 ps. Furthermore, the ~628 ps lifetime component can be attributed to the radiative recombination between the electron and the localized hole, according to our previous OTA and PL results.[22] As for the other two lifetime components of ~11.4 and 81 ns, they might be assigned to be the nonradiative recombination between the electron and self-trapped hole by emitting multiple phonons via two different pathways, in which the self-trapped hole is directly recombined by the electron or it is first detrapped and then recombined by the electron. Besides sharing those lifetime components (~628 ps (18%),

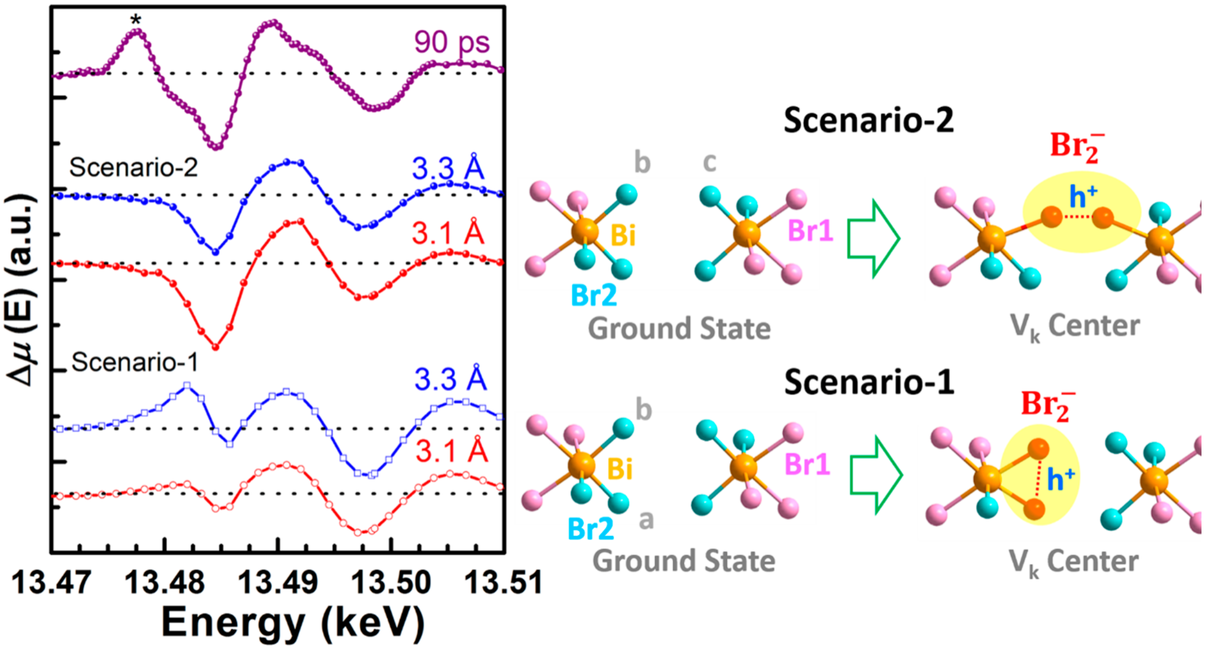

Figure 6. Comparison between experimental Br K-edge XTA spectrum of $Cs_3Bi_2Br_9$ perovskite at Δt = 90 ps and FEFF9 calculated ones in two scenarios, where the Br_2^- dimer (V_k center) are formed by moving two adjacent Br atoms from a same $[BiBr_6]$ unit (Scenario-1) or two neighboring $[BiBr_6]$ units (Scenario-2) in the unit cell (see Figure S3 in the Supporting Information). The distance between two nearest Br ions is ~3.9 Å in the ground state. As for the Br_2^- dimer (V_k center) formation, the distance of ~3.1−3.3 Å between two Br atoms in Scenario-2 was found to best simulate experimental XTA spectrum at 90 ps. The first positive peak (denoted by an asterisk, *) for the electronic change due to the hole self-trapping in the experimental XTA spectrum cannot be reproduced from the FEFF9 simulations, because of the deficiency of FEFF9.

~11.4 ns (40%), and ~81.0 ns (8%)) detected at peak "(a)", the fitting of kinetics at peak "(f)" requires an extra long lifetime component of 59.2 ± 4.2 μs (34%), suggesting the existence of an slow, structural distorted intermediate state after charge recombination. To ensure that the XTA kinetics for self-trapping hole relaxation at Br atom really represents the accomplishment of charge carrier relaxation in the sample, we extended the measuring time window of OTA to the μs range, using ns-OTA spectroscopy to get the recombination dynamics of photoexcited charge carriers. As shown in Figure 4, the ns-OTA recovery kinetics fitted by a multiple exponential model (red curve) with an Gaussian IRF of ~1 ns (fwhm) reveals three lifetime components: 0.7 ± 0.1 ns (super fast < IRF), 8.8 ± 0.4 ns, and 81.2 ± 4.8 ns. The two long lifetime components (8.8 and 81.2 ns) are agreeable with those measured in XTA kinetics, suggesting that the charge is completely gone in the NC system after the self-trapped hole at the Br center disappears. The missing ~59.2 μs component in ns-OTA for distorted structural recovery implies that the slow structural relaxation is optically dark.

A photocycle with three stages is proposed based on our study (Figure 5a). The initially photoexcited state in the $Cs_3Bi_2Br_9$ NC first evolves into a hole self-trapped state around Br atoms within <10 ps (stage II). It then decays to a long-lived structural distorted state without trapped holes (stage III). The hole self-trapping by forming the halide dimer (X_2^-, namely, the V_k center) between two nearest-neighbor halide anions (X^-) is a well-established process ($2X^- + h^+ = X_2^-$) in metal halide crystals.[29−32] Recent theoretical and experimental results of charge carrier distribution in 3D[17,18,33,34] and 2D[16,35−37] LHPs have also revealed that it is more energetically favorable for the hole to be similarly self-trapped as a form of X_2^-. Hence, given the similarity in band-edge composition between $Cs_3Bi_2Br_9$ (Figure 1a) and 2D LHPs,[16] we are tempted to assign the hole self-tapping state (stage II) as the Br_2^- (V_k center) intermediate. A series of XTA spectra were calculated using the FEFF9 based on the formation of a transient V_k center (stage II). By moving two Br atoms from two adjacent $[BiBr_6]$ units in a unit cell closer by 0.6−0.8 Å (Scenario-2; see details given in the Supporting Information and Figure 6), corresponding to a Br−Br distance of 3.3−3.1 Å in the V_k center, the simulated XTA spectra agree best with the experimental XTA spectrum measured at Δt = 90 ps. The optimized Br−Br distance (3.3 to 3.1 Å) for V_k center formation from the simulation is also consistent with that reported in literatures.[34,38]

Since self-trapped holes nonradiatively recombine with electrons via emitting multiple phonons (stage II to III), the atomic rearrangement occurs around Br sites, evidenced by the red shift of feature "(f)" and at 13.5034 keV in XTA spectra from Δt = 90 ps to 100 ns (see Figure S8 in the Supporting Information). After the charge recombination accomplishes, XTA spectra show only amplitude reduction, without further energy shift (Figure S8), which indicates no other detectable intermediate state between stages III and I. Since a long lifetime component of ~59 μs has been observed from stage III to stage I, it is reasonable to speculate that the close Br atoms at stage III finally return to their initial positions at GS (stage I) via thermally jumping over an energy barrier (Figure 5b), in order to minimize the global energy of the entire NC system. The transition rate (τ^{-1}) can be described by the Arrhenius equation,[39,40]

$$\tau^{-1} = \tau_0^{-1} \exp\left(-\frac{\Delta G}{k_B T}\right)$$

where ΔG is the energy barrier between these two stages (Figure 5b), τ_0^{-1} the vibrational frequency of the Br atom, k_B

the Boltzmann constant, and T the temperature. To estimate ΔG, we calculated the phonon density of states (PDOS) of the Br atom versus its vibration frequency by projecting the phonon band structure of $Cs_3Bi_2Br_9$ bulk (see Figure S9 in the Supporting Information). As shown in Figure 5c, the Br atom mainly vibrates beetween the ranges of 0.5−2.8 THz and 4.0−5.7 THz, giving an amplitude-average frequency of 2.7 THz. Using τ^{-1} = 16.9 kHz (∼59 μs^{-1}) and τ_0^{-1} = 2.7 THz, the average ΔG is estimated to be ∼0.485 eV at room temperature. These Br-dominated modes are localized eigenstates (Figure S9), among which the optically active modes, such as rocking and rotating modes,[41] could facilitate the formation of Br_2^- dimer (V_k center) via strong coupling with charge carriers.

The structural dynamics of NCs may be different from that of the bulk material, because of the high surface-area-to-volume ratio in NCs. However, considering that the exciton behavior of $Cs_3Bi_2Br_9$ as a layered form of the vacancy-ordered lead-free perovskites is dominated by its own 2D natural quantum wells,[22,41] we expected that the structure and charge carrier dynamics findings here for $Cs_3Bi_2Br_9$ NCs may also be applied to their bulk counterparts.

■ CONCLUSION

This work demonstrates the great potential of using XTA to directly visualize charge and structure evolution of photoexcited perovskite materials, which is a critical step in understanding the fundamental mechanism that governs their performance. We have observed the photoinduced small polaron formation in lead-free perovskites and have discovered that structural and electronic dynamics of small polarons in perovskites are not necessarily synchronized and could differ in lifetimes by up to several orders of magnitude. The ultra-long-lived structural distortion may lead to an equilibrium long-range disorder of the lattices under continuous light irradiation as a transient “background state”, altering charge carrier transport characteristics. The results from this study can further supply one possible structural interpretation for the current density-voltage (J−V) hysteresis and photodegradation/fast-healing of perovskite solar cells, which are believed to be correlated with the slow structural relaxation to the initial state.[15,42]

■ ASSOCIATED CONTENT

Ⓢ Supporting Information

The Supporting Information is available free of charge on the ACS Publications website at DOI: 10.1021/jacs.9b04557.

> Sample preparation and characterizations, theoretical computation methods and data including DFT for electronic and phonon structures, pump flux and average exciton number, FEFF-simulated XTA spectra, photothermal effect and ORCA for near-edge electronic transition in XA (PDF)

■ AUTHOR INFORMATION

Corresponding Authors

*E-mail address: xyzhang@aps.anl.gov (X.-Y. Zhang)
*E-mail addresses: kaibo.zheng@chemphys.lu.se, kzheng@kemi.dtu.dk (K. Zheng).

ORCID

Elif Ertekin: 0000-0002-7816-1803
David Gosztola: 0000-0003-2674-1379
Jier Huang: 0000-0002-2885-5786
Bin Yang: 0000-0001-9583-921X
Keli Han: 0000-0001-9239-1827
Sophie E. Canton: 0000-0003-4337-8129
Qingyu Kong: 0000-0001-5053-4543
Kaibo Zheng: 0000-0002-7236-1070
Xiaoyi Zhang: 0000-0001-9732-1449

Notes

The authors declare no competing financial interest.

■ ACKNOWLEDGMENTS

This work was supported by the U.S. Department of Energy, Office of Science, Office of Basic Energy Sciences, under Contract No. DE-AC02-06CH11357. Y.W. thanks the support from China Scholarship Council. S.E.C. acknowledges funding from the Helmholtz Recognition Award. The ELI-ALPS project (GINOP-2.3.6-15-2015-00001) is supported by the European Union and cofinanced by the European Regional Development Fund. T.Z. and E.E. are thankful for the grant from NSF (No. PIRE 1545907). S.Y. and J.H. acknowledge the funding from NSF Career Award (DMR) No. 1654140. B.Y. and K.H. are thankful for the support from the National Natural Science Foundation of China (Grant No. 21533010). K.Z. acknowledges the support from Danish Council for Independent Research (No. 7026-0037B) and te Swedish Research Council (No. 2017-05337). The laser system at 11-ID-D of APS were funded through New Facility and Midscale Instrumentation grants to Chemical Sciences and Engineering Division, Argonne National Laboratory (PI: Lin X. Chen). This research used resources of the Advanced Photon Source and the Center for Nanoscale Materials, U.S. Department of Energy (DOE) Office of Science User Facilities operated for the DOE Office of Science by Argonne National Laboratory (under Contract No. DE-AC02-06CH11357).

■ REFERENCES

(1) Burschka, J.; Pellet, N.; Moon, S.-J.; Humphry-Baker, R.; Gao, P.; Nazeeruddin, M. K.; Grätzel, M. Sequential Deposition as a Route to High-Performance Perovskite-Sensitized Solar Cells. *Nature* **2013**, *499* (7458), 316−319.

(2) Lee, M. M.; Teuscher, J.; Miyasaka, T.; Murakami, T. N.; Snaith, H. J. Efficient Hybrid Solar Cells Based on Meso-Superstructured Organometal Halide Perovskites. *Science* **2012**, *338*, 643−647.

(3) Yang, W. S.; Park, B.-W.; Jung, E. H.; Jeon, N. J.; Kim, Y. C.; Lee, D. U.; Shin, S. S.; Seo, J.; Kim, E. K.; Noh, J. H.; Seok, S. I. Iodide Management in Formamidinium-Lead-Halide-Based Perovskite Layers for Efficient Solar Cells. *Science* **2017**, *356* (6345), 1376−1379.

(4) Jeon, N. J.; Na, H.; Jung, E. H.; Yang, T.-Y.; Lee, Y. G.; Kim, G.; Shin, H.-W.; Seok, S. I.; Lee, J.; Seo, J. A Fluorene-Terminated Hole-Transporting Material for Highly Efficient and Stable Perovskite Solar Cells. *Nat. Energy* **2018**, *3*, 682−689.

(5) Babayigit, A.; Ethirajan, A.; Muller, M.; Conings, B. Toxicity of Organometal Halide Perovskite Solar Cells. *Nat. Mater.* **2016**, *15* (3), 247−251.

(6) Aristidou, N.; Sanchez Molina, I.; Chotchuangchutchaval, T.; Brown, M.; Martinez, L.; Rath, T.; Haque, S. A. The Role of Oxygen in the Degradation of Methylammonium Lead Trihalide Perovskite Photoactive Layers. *Angew. Chem.* **2015**, *127* (28), 8326−8330.

(7) Maughan, A. E.; Ganose, A. M.; Bordelon, M. M.; Miller, E. M.; Scanlon, D. O.; Neilson, J. R. Defect Tolerance to Intolerance in the Vacancy-Ordered Double Perovskite Semiconductors Cs_2SnI_6 and Cs_2TeI_6. *J. Am. Chem. Soc.* **2016**, *138* (27), 8453−8464.

(8) Zhao, Z.; Gu, F.; Li, Y.; Sun, W.; Ye, S.; Rao, H.; Liu, Z.; Bian, Z.; Huang, C. Mixed Organic Cation Tin Iodide for Lead Free

Perovskite Solar Cells with an Efficiency of 8.12%. *Adv. Sci.* **2017**, *4* (11), 1700204.

(9) Liang, L.; Gao, P. Lead Free Hybrid Perovskite Absorbers for Viable Application: Can We Eat the Cake and Have It Too? *Adv. Sci.* **2018**, *5* (2), 1700331.

(10) Giustino, F.; Snaith, H. J. Toward Lead-Free Perovskite Solar Cells. *ACS Energy Lett.* **2016**, *1* (6), 1233−1240.

(11) McCall, K. M.; Stoumpos, C. C.; Kostina, S. S.; Kanatzidis, M. G.; Wessels, B. W. Strong Electron-Phonon Coupling and Self-Trapped Excitons in the Defect Halide Perovskites $A_3M_2I_9$ (A = Cs, Rb; M = Bi, Sb). *Chem. Mater.* **2017**, *29* (9), 4129−4145.

(12) Hao, F.; Stoumpos, C. C.; Cao, D. H.; Chang, R. P.; Kanatzidis, M. G. Lead-Free Solid-State Organic-Inorganic Halide Perovskite Solar Cells. *Nat. Photonics* **2014**, *8* (6), 489.

(13) Maughan, A. E.; Ganose, A. M.; Candia, A. M.; Granger, J. T.; Scanlon, D. O.; Neilson, J. R. Anharmonicity and Octahedral Tilting in Hybrid Vacancy-Ordered Double Perovskites. *Chem. Mater.* **2018**, *30* (2), 472−483.

(14) Park, B. W.; Philippe, B.; Zhang, X.; Rensmo, H.; Boschloo, G.; Johansson, E. M. Bismuth Based Hybrid Perovskites $A_3Bi_2I_9$ (A: Methylammonium or Cesium) for Solar Cell Application. *Adv. Mater.* **2015**, *27* (43), 6806−6813.

(15) Nie, W.; Blancon, J.-C.; Neukirch, A. J.; Appavoo, K.; Tsai, H.; Chhowalla, M.; Alam, M. A.; Sfeir, M. Y.; Katan, C.; Even, J.; Tretiak, S.; Crochet, J. J.; Gupta, G.; Mohite, A. D. Light-Activated Photocurrent Degradation and Self-Healing in Perovskite Solar Cells. *Nat. Commun.* **2016**, *7*, 11574.

(16) Cortecchia, D.; Yin, J.; Bruno, A.; Lo, S.-Z. A.; Gurzadyan, G. G.; Mhaisalkar, S.; Brédas, J.-L.; Soci, C. Polaron Self-Localization in White-Light Emitting Hybrid Perovskites. *J. Mater. Chem. C* **2017**, *5* (11), 2771−2780.

(17) Kang, B.; Biswas, K. Shallow Trapping Vs. Deep Polarons in a Hybrid Lead Halide Perovskite, $CH_3NH_3PbI_3$. *Phys. Chem. Chem. Phys.* **2017**, *19* (40), 27184−27190.

(18) Neukirch, A. J.; Nie, W.; Blancon, J.-C.; Appavoo, K.; Tsai, H.; Sfeir, M. Y.; Katan, C.; Pedesseau, L.; Even, J.; Crochet, J. J.; Gupta, G.; Mohite, A. D.; Tretiak, S. Polaron Stabilization by Cooperative Lattice Distortion and Cation Rotations in Hybrid Perovskite Materials. *Nano Lett.* **2016**, *16* (6), 3809−3816.

(19) Miyata, K.; Meggiolaro, D.; Trinh, M. T.; Joshi, P. P.; Mosconi, E.; Jones, S. C.; De Angelis, F.; Zhu, X.-Y. Large Polarons in Lead Halide Perovskites. *Sci. Adv.* **2017**, 3 (8), No. e1701217.

(20) Park, M.; Neukirch, A. J.; Reyes-Lillo, S. E.; Lai, M.; Ellis, S. R.; Dietze, D.; Neaton, J. B.; Yang, P.; Tretiak, S.; Mathies, R. A. Excited-State Vibrational Dynamics toward the Polaron in Methylammonium Lead Iodide Perovskite. *Nat. Commun.* **2018**, *9* (1), 2525.

(21) Zheng, K.; Abdellah, M.; Zhu, Q.; Kong, Q.; Jennings, G.; Kurtz, C. A.; Messing, M. E.; Niu, Y.; Gosztola, D. J.; Al-Marri, M. J.; et al. Direct Experimental Evidence for Photoinduced Strong-Coupling Polarons in Organolead Halide Perovskite Nanoparticles. *J. Phys. Chem. Lett.* **2016**, *7* (22), 4535−4539.

(22) Yang, B.; Chen, J.; Hong, F.; Mao, X.; Zheng, K.; Yang, S.; Li, Y.; Pullerits, T.; Deng, W.; Han, K. Lead Free, Air Stable All Inorganic Cesium Bismuth Halide Perovskite Nanocrystals. *Angew. Chem.* **2017**, *129* (41), 12645−12649.

(23) Uno, K.; Notoya, Y.; Fujikawa, T.; Yoshikawa, H.; Nishikawa, K. Br K-Edge X-Ray Absorption near Edge Structure Analyses of Bromine Residue Carbon Compounds Using Full Multiple-Scattering Theory. *Jpn. J. Appl. Phys.* **2005**, *44* (6R), 4073.

(24) Morawitz, H.; Bagus, P.; Clarke, T.; Gill, W.; Grant, P.; Street, G. B. X-Ray Absorption in Polymers. *Synth. Met.* **1979/80**, *1*, 267−278.

(25) Santomauro, F. G.; et al. Localized holes and delocalized electrons in photoexcited inorganic perovskites: Watching each atomic actor by picosecond X-ray absorption spectroscopy. *Struct. Dyn.* **2017**, *4*, 044002.

(26) Koningsberger, D. C.; Prins, R. *X-ray Absorption: Principles, Applications, Techniques of EXAFS, SEXAFS and XANES*; John Wiley & Sons: New York, 1988.

(27) Stern, E. A.; Heald, S. M.; Koch, E. E. *Principles and Applications of EXAFS*; North-Holland: Amsterdam, 1983.

(28) Bunker, G. B. *An X-ray Absorption Study of Transition Metal Oxides*; University of Washington, Seattle, WA, 1984.

(29) Williams, R. T.; Song, K. S. The self-Trapped Exciton. *J. Phys. Chem. Solids* **1990**, *51* (7), 679−716.

(30) Castner, T. G.; Känzig, W. The Electronic Structure of V-Centers. *J. Phys. Chem. Solids* **1957**, *3* (3−4), 178−195.

(31) Iwanaga, M.; Azuma, J.; Shirai, M.; Tanaka, K.; Hayashi, T. Self-Trapped Electrons and Holes in $PbBr_2$ Crystals. *Phys. Rev. B: Condens. Matter Mater. Phys.* **2002**, *65* (21), 214306.

(32) Stoneham, A. M.; Gavartin, J.; Shluger, A. L.; Kimmel, A. V.; Ramo, D. M.; Rønnow, H. M.; Aeppli, G.; Renner, C. Trapping, Self-Trapping and The Polaron Family. *J. Phys.: Condens. Matter* **2007**, *19*, 255208.

(33) Peng, C.; Wang, J.; Wang, H.; Hu, P. Unique Trapped Dimer State of the Photogenerated Hole in Hybrid Orthorhombic $CH_3NH_3PbI_3$ Perovskite: Identification, Origin, and Implications. *Nano Lett.* **2017**, *17* (12), 7724−7730.

(34) Whalley, L. D.; Crespo-Otero, R.; Walsh, A. H-Center and V-Center Defects in Hybrid Halide Perovskites. *ACS Energy Lett.* **2017**, *2* (12), 2713−2714.

(35) Yin, J.; Li, H.; Cortecchia, D.; Soci, C.; Brédas, J.-L. Excitonic and Polaronic Properties of 2D Hybrid Organic-Inorganic Perovskites. *ACS Energy Lett.* **2017**, *2* (2), 417−423.

(36) Smith, M. D.; Karunadasa, H. I. White-Light Emission from Layered Halide Perovskites. *Acc. Chem. Res.* **2018**, *51* (3), 619−627.

(37) Cortecchia, D.; Yin, J.; Petrozza, A.; Soci, C. White Light Emission in Low-Dimensional Perovskites. *J. Mater. Chem. C* **2019**, *7*, 4956−4969.

(38) Tasker, P.; Stoneham, A. An Appraisal of the Molecular Model for the V_k Centre. *J. Phys. Chem. Solids* **1977**, *38* (10), 1185−1189.

(39) Nagaosa, N.; Ogawa, T. Theory of Photoinduced Structure Changes. *Phys. Rev. B: Condens. Matter Mater. Phys.* **1989**, *39* (7), 4472.

(40) Shimakawa, K.; Kolobov, A.; Elliott, S. Photoinduced Effects and Metastability in Amorphous Semiconductors and Insulators. *Adv. Phys.* **1995**, *44* (6), 475−588.

(41) Bass, K. K.; Estergreen, L.; Savory, C. N.; Buckeridge, J.; Scanlon, D. O.; Djurovich, P. I.; Bradforth, S. E.; Thompson, M. E.; Melot, B. C. Vibronic Structure in Room Temperature Photoluminescence of the Halide Perovskite $Cs_3Bi_2Br_9$. *Inorg. Chem.* **2017**, *56* (1), 42−45.

(42) Tsai, H.; Asadpour, R.; Blancon, J.-C.; Stoumpos, C. C.; Durand, O.; Strzalka, J. W.; Chen, B.; Verduzco, R.; Ajayan, P. M.; Tretiak, S.; et al. Light-Induced Lattice Expansion Leads to High-Efficiency Perovskite Solar Cells. *Science* **2018**, *360* (6384), 67−70.